

# Mathematical model of the morphogenesis checkpoint in budding yeast

Andrea Ciliberto,<sup>1</sup> Bela Novak,<sup>2,3</sup> and John J. Tyson<sup>1</sup>

<sup>1</sup>Department of Biology, Virginia Polytechnic Institute and State University, Blacksburg, VA 24061

<sup>2</sup>Molecular Network Dynamics Research Group of Hungarian Academy of Sciences and <sup>3</sup>Department of Agricultural Chemical Technology, Budapest University of Technology and Economics, H-1521 Budapest, Hungary

The morphogenesis checkpoint in budding yeast delays progression through the cell cycle in response to stimuli that prevent bud formation. Central to the checkpoint mechanism is Swe1 kinase: normally inactive, its activation halts cell cycle progression in G2. We propose a molecular network for Swe1 control, based on published observations of budding yeast and analogous control signals in fission yeast. The proposed Swe1 network is merged with a model of cyclin-dependent kinase regulation, converted into a set of differential equations and studied by numerical

simulation. The simulations accurately reproduce the phenotypes of a dozen checkpoint mutants. Among other predictions, the model attributes a new role to Hsl1, a kinase known to play a role in Swe1 degradation: Hsl1 must also be indirectly responsible for potent inhibition of Swe1 activity. The model supports the idea that the morphogenesis checkpoint, like other checkpoints, raises the cell size threshold for progression from one phase of the cell cycle to the next.

## Introduction

During the cell division cycle, a cell first replicates its hereditary material (S phase) and then segregates the chromosomes to the newborn daughter cells (mitosis). Alternation of mitosis and DNA replication is necessary for the cycle to be successful: two consecutive rounds of mitosis cause lethal mis-segregation of the genome, and successive rounds of DNA synthesis are usually disadvantageous (Enoch and Nurse, 1991). In molecular terms, the proper order of the events is ensured by the alternation of different Cdk activities (Morgan 1995). Cdk activities are subject to multiple controls: they are activated by binding to cyclins, and they can be inhibited by tyrosine phosphorylation or by stoichiometric binding with a Cdk inhibitor (Sic1 in budding yeast). Waves of different classes of cyclins alternate during the cycle, and the resulting Cdk–cyclin complexes are responsible for various cell cycle events. In budding yeast (where the cell-cycle regulating Cdk is Cdc28), the first complex to arise during the cycle is Cdc28–Cln3, which senses growth of the cell in G1, followed by Cdc28–Cln1 and Cdc28–Cln2, which are responsible for bud initiation and spindle pole body duplication. They are

followed by Cdc28–Clb5 and Cdc28–Clb6, which are primarily responsible for S phase, and finally by the mitotic complexes Cdc28–Clb1 and Cdc28–Clb2.

The main transitions of the cell division process—the onset of DNA replication (Start), entry into mitosis (G2-M transition), and exit from mitosis—are controlled by surveillance mechanisms, also known as checkpoints (Hartwell and Weinert, 1989). The G2-M checkpoint plays a major role in fission yeast (*Schizosaccharomyces pombe*), where it forestalls mitosis until the cell grows to a critical size and properly replicates its DNA (Nurse, 1999). The molecular events which control this transition are the inhibitory phosphorylation of tyrosine-15 of Cdc2 (the fission yeast homologue of Cdc28), executed by the protein kinase Wee1, and the activating dephosphorylation of this site, catalyzed by the phosphatase Cdc25. If DNA is damaged or not properly replicated, the checkpoint is engaged, Cdc2 is phosphorylated on tyrosine-15, and cell cycle progression is halted. The inhibitory phosphorylation is relieved when DNA is fully replicated or the damage is repaired (Enoch and Nurse, 1991).

Budding yeast contains homologues of Wee1 and Cdc25, known respectively as Swe1 kinase (Booher et al., 1993) and Mih1 phosphatase (Russell et al., 1989). But in budding yeast, Mih1 and Swe1 are not used to check cell size, nor are

The online version of this article contains supplemental material.

Address correspondence to John J. Tyson, Dept. of Biology, M.C. 0406, Virginia Polytechnic Institute and State University, Blacksburg, VA 24061. Tel.: (540) 231-4662. Fax: (540) 231-9307. email: tyson@vt.edu

Key words: molecular networks; dynamical systems; cell cycle; size control; Swe1 kinase

Abbreviations used in this paper: MPF, M-phase promoting factor; ND, nuclear division.

Table I. Comparing experiments and simulations

Genotypes	Parameters	Cell cycle properties		Nuclear division time					
				$\alpha$ -factor		cdc24 <sup>ts</sup> $\alpha$ -factor		cdc24 <sup>ts</sup> elutriation	
				E	S	E	S	E	S
Wild type			CT = 139 mab = 0.8 mad = 1.6	65–75 <sup>a,b</sup>	79	135–160 <sup>a,b</sup>	150	250 <sup>a</sup>	225
<i>swe1</i> $\Delta$	$k_{s,swe} = 0$	same size and cycle as wild type <sup>c</sup>	CT = 139 mab = 0.8 mad = 1.6		79	80 <sup>a,d</sup>	79	145 <sup>a</sup>	131
<i>mih1</i> $\Delta$	$k_{s,mih1} = 0$	G2 delay and cells 15% bigger than wild type <sup>c,e</sup>	CT = 139 mab = 0.8 mad = 1.6	80 <sup>a</sup>	82	G2 block <sup>a</sup>	G2 block	>300 <sup>a</sup>	G2 block
<i>hsl1</i> $\Delta$	$k_{hsl1} = 0$	same as wt <sup>d</sup>	CT = 139 mab = 0.8 mad = 1.7		81	165 <sup>d</sup>	171		255
<i>mih1</i> $\Delta$ <i>hsl1</i> $\Delta$	$k_{hsl1} = 0$ $k_{s,mih1} = 0$	G2 arrest <sup>d</sup>	G2 block		G2 block		G2 block		G2 block
<i>mih1</i> $\Delta$ <i>swe1</i> $\Delta$	$k_{s,swe} = 0$ $k_{s,mih1} = 0$	same size and cycle as wild type <sup>d</sup>	CT = 139 mab = 0.8 mad = 1.6		79		79		131
<i>clb2</i> $\Delta$ <i>mih1</i> $\Delta$	$k_{s,clb2} = 0.005$ $k_{mih1} = 0$	elongated cells, G2 delay <sup>f</sup>	CT = 139 mab = 2.1 mad = 4.2		105		G2 block		G2 block
<i>clb2</i> $\Delta$ <i>hsl1</i> $\Delta$	$k_{s,clb2} = 0.005$ $k_{hsl1} = 0$	elongated cells (longer than <i>clb2</i> $\Delta$ <i>mih1</i> $\Delta$ ), G2 delay <sup>f</sup>	CT = 139 mab = 2.5 mad = 5.1		105		G2 block		G2 block
<i>GAP-SWE1</i>	$k_{s,swe} = 0$ $k_{s,sweC} = 0.001$		CT = 139 mab = 0.8 mad = 1.6	75 <sup>a</sup>	79	118 <sup>a</sup>	118		163
<i>GAL-SWE1</i>	$k_{s,swe} = 0$ $k_{s,sweC} = 2.5$	G2 block <sup>c</sup>	G2 block		G2 block		G2 block		G2 block
<i>swe1-SWE1</i> <i>MIH1-MIH1</i>	$k_{s,swe} = 0.00125$		CT = 139 mab = 0.8 mad = 1.6		79		94	190 <sup>a</sup>	150
<i>SWE1-SWE1</i> <i>MIH1-mih1</i>	$k_{s,mih1} = 0.05$		CT = 139 mab = 0.8 mad = 1.6		79		299	385 <sup>a</sup>	368
<i>SWE1-2X</i>	$k_{s,swe} = 0.005$	same as wt <sup>g</sup>	CT = 139 mab = 0.8 mad = 1.6		79	330 <sup>d</sup>	381		445
<i>SWE1-4X</i>	$k_{s,swe} = 0.01$		CT = 139 mab = 0.8 mad = 1.6		79	>300 <sup>d</sup>	>300		G2 block

The first column catalogs genotypes and changes of parameter values compared to the wild type (Table S2). In the second column, experimental (E) observations of exponentially growing cells are compared with simulated (S) cell cycles in terms of mass at division (mad), mass at birth (mab), and cycle time (CT, min). The third column, comprised of three sub-columns, shows a comparison between experimental nuclear division (ND) times and simulations. In the sub-columns are collected ND data measured in different conditions: in cells grown after synchronization by  $\alpha$ -factor arrest and release, in cells synchronized with the same method and grown in *cdc24<sup>ts</sup>* mutants at restrictive temperature (same parameters as wild type, except for  $k'_{mih} = 0.5$ ,  $k'_{mih} = 0.05$ , and  $k_{hsl1} = 0$ , i.e., checkpoint engaged), and finally in cells synchronized by elutriation and grown in *cdc24<sup>ts</sup>* mutants at restrictive temperature.

<sup>a</sup>Sia et al., 1996.

<sup>b</sup>Sia et al., 1998.

<sup>c</sup>Booher et al., 1993.

<sup>d</sup>McMillan et al., 1999a; ND in *SWE1-2X* extrapolated from Fig. 3.

<sup>e</sup>Russell et al., 1989.

<sup>f</sup>Lew, D.J., personal communication.

<sup>g</sup>McMillan et al., 1998.

they involved in monitoring DNA replication, as evidenced by the fact that cells containing a mutant form of Cdc28 lacking the tyrosine phosphorylation site are still perfectly viable in the presence of inhibitors of DNA synthesis (Amon et al., 1992; Sorger and Murray, 1992). Recently, Lew and coworkers have shown in an elegant series of papers that these tyrosine phosphorylation–dephosphorylation reactions in budding yeast are involved in a different kind of check-

point, called the morphogenesis checkpoint (for review see Lew, 2000). This surveillance mechanism halts cell cycle progression when bud formation is impaired, which is a plausible event for yeast cells growing in natural conditions because several external stimuli (such as heat shock and osmotic shock) are able to arrest or delay the formation of a bud (Sia et al., 1998). By arresting or delaying cell cycle progression, the morphogenesis checkpoint prevents formation

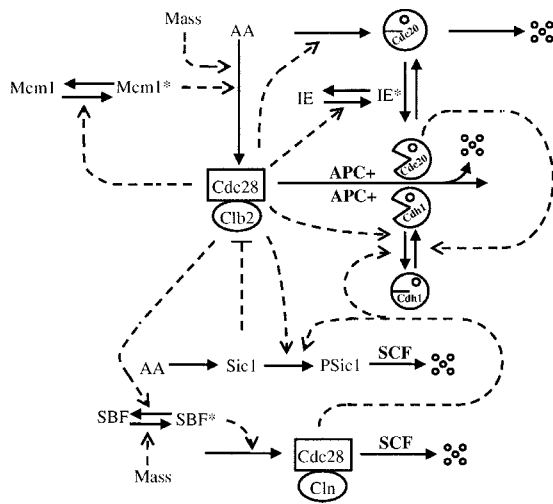


Figure 1. **Molecular mechanism of the cell-cycle engine in budding yeast.** AA, amino acids; APC, anaphase promoting complex; Cdc20 and Cdh1, proteins that target Clb2 to the APC; Cln, G1 cyclins; IE, intermediary enzyme; Mcm1, transcription factor for Clb2; SBF, transcription factor for Cln; SCF, Skp1–Cdc53–F-box protein complex; Sic1, stoichiometric inhibitor of Cdc28–Clb2; five small-circles, degradation fragments. Notice that Cdc28–Clb2 has two major antagonists, Sic1 and Cdh1. In G1 phase, Sic1 and Cdh1 are active and Cdc28–Clb2 is repressed, and vice versa in S-G2-M. Cln-dependent kinase activity pushes the engine from G1 to S-G2-M by inactivating Sic1 and Cdh1. Cln synthesis turns on when the cell grows to a critical size, because Mass activates SBF. The transition from S-G2-M back to G1 is driven by Cdc20, which targets Clb2 for degradation and (indirectly) activates Cdh1. For further details, see Tyson and Novak (2001) and Chen et al. (2000). The asterisk identifies the more active form of a protein.

of dinucleated cells, which are less viable than mononucleated cells (Sia et al., 1996). The arrest is not complete; after several hours, unbudded cells undergo mitosis (called “adaptation”) and become dinucleate (Sia et al., 1996).

In this paper, we propose a molecular network for the morphogenesis checkpoint, based largely on Lew’s work (Lew, 2000), and we translate it into a set of differential equations. Our main goal is to explain the observed properties of cells under checkpoint-free and checkpoint-induced conditions in terms of the temporal dynamics of the underlying molecular regulatory system. The model provides a common framework for describing many diverse features of the checkpoint; not only G2 delay, but also adaptation and cell death. The model also suggests a number of experiments that would be especially revealing about the molecular regulatory system.

## Results

### A mathematical model

In Table I and online supplemental material (Experimental basis of the model, available at <http://www.jcb.org/cgi/content/full/jcb.200306139/DC1>), we summarize the experimental results that support a hypothetical molecular mechanism for the morphogenesis checkpoint, based on posttranslational modification of Swe1. Obviously, the checkpoint mechanism cannot be separated from the whole

network of cell-cycle regulatory proteins. Cdc28–Clb2 is the key regulator of mitosis and as such it is the main target of Swe1 kinase activity, but there are other connections. For example, the transcription factor SBF controls Swe1 expression as well as Cln1-2 expression; and bud formation, needed for Hsl1 activation, is due to Cdc28–Cln1-2. Therefore, if we want to model the morphogenesis checkpoint, we must start with a model of the cell cycle engine.

**Cell cycle engine.** Tyson and Novak (2001) have proposed a simplified version (Fig. 1) of a model by Chen et al. (2000) of the budding yeast cell cycle. In the Tyson-Novak model, Cln1, Cln2, Clb5, and Clb6 are lumped together as “Cln”, and Clb1 and Clb2 are lumped together as “Clb2”. Cln synthesis is due to SBF, and therefore is a function of cell size (Dirick et al., 1995). Cln-dependent kinase activity induces degradation of Sic1, and initiates DNA synthesis (via Clb5-6). Moreover, Cln-dependent kinase activity inactivates Cdh1, permitting Clb2 level to rise. Cdc28–Clb2 activity, relieved from Sic1 and Cdh1 inhibition, turns on its own transcription through Mcm1, and turns off Cln transcription by inhibiting SBF. The cell enters into M phase, and Cdc28–Clb2 starts a negative feedback loop by activating a putative intermediate enzyme, and by enhancing Cdc20 transcription. The ultimate effect of the loop is to activate the anaphase promoting complex, which degrades Clb2 and drives the cell out of mitosis.

In addition to Mcm1-dependent transcription of *CLB2*, we assume a background transcription rate, independent of Mcm1. After Tyson and Novak (2001), we assume that the rate of Clb2 synthesis increases with cell size ( $M$ ), and eventually saturates. This relationship mimics the accumulation of Clb2 in the nucleus as the cell grows. To this engine, we now graft our mechanism for the morphogenesis checkpoint (Fig. 2).

**Hsl1-Hsl7-Bud.** To keep the model simple, while preserving its main biological properties, we do not take into account any spatial features; first, we assume simply that bud formation is turned on by the Clns (see Other rules). Second, we do not keep track of Hsl1 synthesis, degradation, and activation. Because Hsl1 activation depends on bud presence, we assume that when the bud is formed, Hsl1 is able to “modify” Swe1 (Swe1M denotes the modified form of Swe1). The nature of this modification is not clear, as Swe1 does not appear to be a substrate for Hsl1 (Cid et al., 2001; Theesfeld et al., 2003). Whatever the modification may be, we assume that it does not affect Swe1 stability but makes Swe1 inactive (0.5% of the fully active form). Finally, we ignore Hsl7 because Hsl1 catalyzes the rate-limiting step for Swe1 modification (McMillan et al., 1999a). Many other proteins are involved in this step (septins, Kcc4, Gin4, Cla4, and Nap1), but again, as a first approximation, we ignore them.

**Swe1.** Swe1 does not play a major role during the normal cell cycle of *S. cerevisiae* even though it is able to phosphorylate Cdc28 on tyrosine-19 (Booher et al., 1993). The cell cycle is perfectly normal in *swe1Δ* (Booher et al., 1993). Nonetheless, Swe1 can affect cell cycle progression, as *swe1Δ* cells are slightly smaller than wild-type cells (Harvey and Kellogg, 2003), and Swe1 overexpression (*GAL-SWE1*, wild-type gene controlled by a GAL promoter) leads to a G2 block and very elongated buds (Booher et al., 1993).

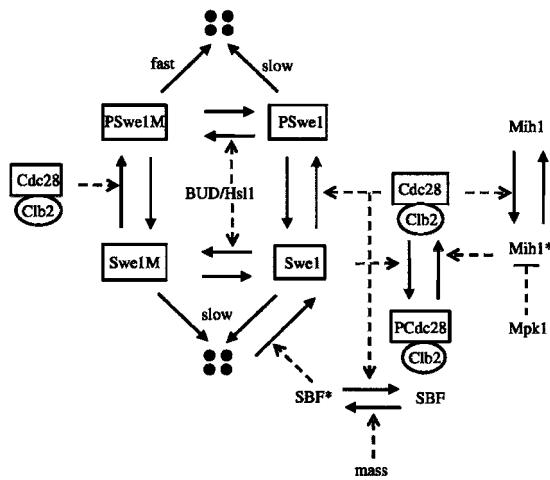


Figure 2. **The Swe1 box.** Swe1 can be present in four different forms during the cell cycle: unchanged (Swe1), phosphorylated by Cdc28–Clb2 (PSwe1); or modified by Hsl1 (Swe1M) or both (PSwe1M). The doubly modified form we assume to be less stable than the others. The unphosphorylated, unmodified form of Swe1 is assumed to be most active in phosphorylating Cdc28–Clb2. Cdc28 is dephosphorylated by Mih1. We assume that Cdc28–Clb2 phosphorylates and activates Mih1, and MAPK (Mpk1) inactivates Mih1. The asterisk identifies the more active form of a protein.

Cdc28–Clb2 phosphorylates Swe1 *in vitro* (McMillan et al., 2002), and we assume that Cdc28–Clb2 catalyzes the same reaction *in vivo* (we call the phosphorylated form PSwe1). We assume that PSwe1 has 10% of Swe1 kinase activity.

Swe1 is degraded by proteasomes, after polyubiquitination by the Skp1–Cdc53–F-box protein complex (Kaiser et al., 1998). We assume that Swe1, like other substrates of this complex, must be phosphorylated in order to be ubiquitinated. The phosphorylation we assume to be necessary but not sufficient (i.e., PSwe1 is as stable as Swe1). Efficient degradation of Swe1, we assume, requires modification by both Cdc28–Clb2 and Hsl1 (i.e., PSwe1M is both catalytically inactive and highly unstable).

In the model, Hsl1 and Cdc28–Clb2 act along the same degradation pathway, each introducing a different posttranslational modification in Swe1. Either modification alone renders Swe1 less active, whereas both are needed to make it unstable. Based on recent data (McMillan et al., 2002), we assume that these two modifications can occur in either order, although Hsl1 acts first in wild-type cells. The four different forms (Swe1, Swe1M, PSwe1, and PSwe1M) comprise the “Swe1 box” in Fig. 2.

The antagonistic relationship between Cdc28–Clb2 and Swe1 is at the core of our model of the morphogenesis checkpoint. When the checkpoint is induced, Swe1 phosphorylates and inhibits Cdc28–Clb2 (Booher et al., 1993). (Swe1 can also function as a stoichiometric inhibitor of Cdc28–Clb2 [McMillan et al., 1999b], but we do not keep track of this effect in the model.) On the other hand, Cdc28–Clb2 down-regulates Swe1 in three ways. By phosphorylating Swe1, it reduces Swe1 activity and prepares Swe1 for degradation. In addition, Cdc28–Clb2 inhibits the transcription factor, SBF, and thereby shuts off synthesis of Swe1. If Cdc28–Clb2 successfully down-regulates Swe1,

then the cell proceeds into mitosis. If Swe1 successfully inhibits Cdc28–Clb2, then the cell arrests in G2 phase.

**Mih1.** In frog egg extracts (where the homologues of Mih1 and Cdc28–Clb2 are called Cdc25 and M-phase promoting factor [MPF]), Cdc25 has been shown to be involved in a positive feedback loop with MPF, whereby MPF activates Cdc25 by phosphorylation, and Cdc25 activates MPF by dephosphorylating it (Izumi et al., 1992). Although there are no data to confirm the presence of such a feedback loop in *S. cerevisiae*, we assume it is operational in our model.

**MAPK pathway.** When bud formation fails, Hsl1 is unable to down-regulate Swe1 activity. In addition, a second signaling pathway, operating through a MAPK (Mpk1) is thought to inhibit Mih1 and thereby alter the ratio of Mih1 to Swe1 activities (Harrison et al., 2001). Rather than introduce a full MAPK pathway, we simply assume that the rate constants characterizing Cdc28–Clb2 dephosphorylation by Mih1 are decreased 10-fold as an effect of Mpk1 activation, in response to bud failure.

**Equations and parameters.** The wiring diagrams of Figs. 1 and 2 have been translated into a set of ordinary differential equations (Table S1, available at <http://www.jcb.org/cgi/content/full/jcb.200306139/DC1>) using mass-action kinetics for the most part. Where we use Michaelis-Menten kinetics, we are treating the posttranslational modification as a “Goldbeter-Koshland switch” (Goldbeter and Koshland, 1981), which is a convenient and reasonable way to model information processing in signal transduction pathways. For transcriptional control of Cdc20 synthesis by Cdc28–Clb2, we use a Hill function for convenience; other assumptions would work just as well. The parameter values used in our simulations are shown in Table S2, available at <http://www.jcb.org/cgi/content/full/jcb.200306139/DC1>. Degradation rates for the four different forms of Swe1 have been computed from Sia et al. (1998), whereas those parameter values relative to Fig. 1 are derived from Tyson and Novak (2001). All other parameter values for Fig. 2 have been chosen to fit the experimental data summarized in Table I.

**Other rules.** A nontrivial aspect of modeling gene networks is to link physiological observations with molecular states of the model. Our variables are concentrations, but bud formation, nuclear division (ND) and cell death are the experimental observables. We have adopted the following six rules to relate our calculations to experimental observations: (1) cell size increases exponentially ( $M = M_0 e^{\mu t}$ ,  $\mu$  = specific growth rate). Cell division ( $M \rightarrow M/2$ ) occurs when Cdc28–Clb2 decreases below a threshold,  $[Clb2] = 0.2$ ; (2) we introduce a variable [BE] that represents the extent of phosphorylation of proteins targeted by Cdc28–Cln. We assume that a bud is formed ( $[BUD] = 1$ ) and Hsl1 is activated when [BE] increases above a threshold value (0.6). The bud is removed ( $[BUD] = 0$ ) and Hsl1 is inactivated when the cell divides. We model *hsl1Δ* by setting  $k_{hsl1} = 0$ ; (3) the MAPK signal is modeled by reducing the activity of Mih1 by 90% ( $k_{mih} = 0.5$ ,  $k'_{mih} = 0.05$ ); (4) most experiments report the percentage of cells that undergo ND as a function of time. Because our model is deterministic, all cells divide at the same time. We identify the experimental time when 50% of the cells have undergone ND with the time in the model when anaphase occurs, i.e., when Cdc20

is activated (increases above a threshold value of 0.3); (5) experimentally, cell synchronization is obtained by treating cells for 2–3 h with  $\alpha$ -factor, and then releasing them from the block. We simulate this experiment by allowing growth for 120 min at one half the specific growth rate of normal cells, and setting SBF activity to 0, so that *CLN* and *SWE1* are not transcribed (Sia et al., 1996). The variables at the end of the 120 min simulation are used as the initial conditions for the ND timing experiment. In some experiments, synchronization was obtained by elutriation. In this case, we choose our initial conditions at the minimum mass value of a regular cell cycle; and (6) we use the following rule to determine whether the cell is viable or not: a mononucleated cell (dinucleated cell) is dead if its size exceeds four times (five times) the size of a wild-type cell at division.

### Kinetic data in *cdc24<sup>ts</sup>* background strains

In the laboratory, the morphogenesis checkpoint can be induced by treating cells with inhibitors of actin polymerization (Latrunculin-A [McMillan et al., 1998]), by expressing mutations that interfere with actin polymerization (*tpm1 $\Delta$*  [McMillan et al., 1998]), or with bud formation in general (*cdc24<sup>ts</sup>* [Lew and Reed, 1995]). In this paper, we address only experiments using *cdc24<sup>ts</sup>* mutants (Sia et al., 1996, 1998; McMillan et al., 1999a). A summary of the experimental data used to constrain the model is presented in Table I, together with the corresponding simulation results.

The effect of the morphogenesis checkpoint is commonly measured as a delay of ND in *cdc24<sup>ts</sup>* mutants relative to *CDC24* control cells (Lew and Reed, 1995). In most experiments, yeast cells are synchronized by  $\alpha$ -factor arrest and release, and then, while the cells are growing at the restrictive temperature, the time of the first ND is measured (Sia et al., 1996). ND occurs much later in *cdc24<sup>ts</sup>* cells at the restrictive temperature (checkpoint invoked) than in *CDC24* cells (checkpoint silent). The delay depends, of course, on what other mutations are introduced into the *cdc24<sup>ts</sup>* and *CDC24* strains (Table I).

The basic mutant, *cdc24<sup>ts</sup>* at the restrictive temperature, is unable to develop a bud; nevertheless, it undergoes ND 135–165 min after release from  $\alpha$ -factor (Sia et al., 1996; McMillan et al., 1999a). In other words, the morphogenesis “checkpoint” in this mutant is not very tight; after 2–3 h the cell adapts to it (Sia et al., 1996). The checkpoint depends on Swe1 because *cdc24<sup>ts</sup> swe1 $\Delta$*  does not show any delay of ND compared with wild type (Sia et al., 1996). Mih1 is necessary for adaptation because *cdc24<sup>ts</sup> mih1 $\Delta$*  is irreversibly blocked in G2 (Sia et al., 1996). On the other hand, *cdc24<sup>ts</sup> hsl1 $\Delta$*  does not show a phenotype more severe than *cdc24<sup>ts</sup>*, suggesting that Hsl1 is already inactive in *cdc24<sup>ts</sup>* (McMillan et al., 1999a); not surprisingly because septins, required for full activation of Hsl1, are not properly organized in this mutant.

Finally, we want to explore mutants where Swe1 is overexpressed. Swe1 production can be made constitutive by coupling the *SWE1* gene to either the *GAL* or *GAP* promoter. (Transcriptional efficiency is lower from the *GAP* promoter than from the *GAL* promoter.) *GAL-SWE1* is blocked in G2 phase even when the morphogenesis checkpoint is not active (Booher et al., 1993). In *cdc24<sup>ts</sup> GAP-SWE1*, ND is delayed (118 min) but not as much as in *cdc24<sup>ts</sup>* cells (Sia et al.,

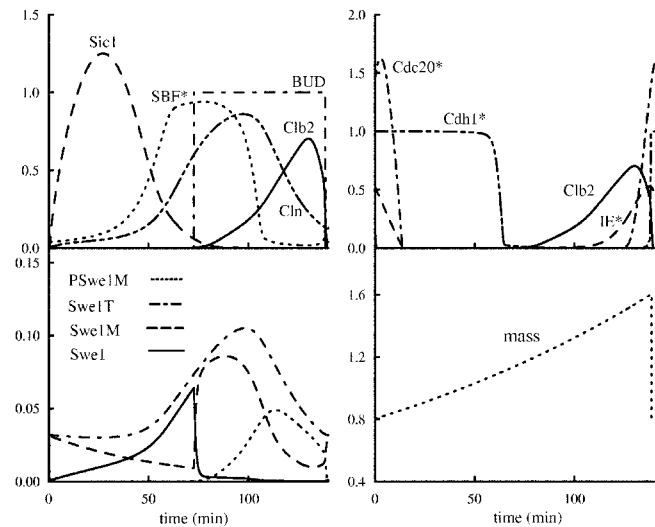


**Figure 3. Time courses of mass and concentrations during the cycle of wild-type cells.** Numerical solution of equations in Table S1, given the parameter values and initial conditions from Table S2. Because Cdc28 is present in excess and binds quickly to cyclins, there are no free cyclins in the model: a curve marked by a cyclin, such as Cln, always refers to the concentration of the relevant complex with Cdc28, such as [Cdc28–Cln]. Swe1T refers to total Swe1 concentration. The concentration of the phosphorylated form of Swe1 is negligible and not depicted. The asterisk identifies the more active form of a protein.

1996). Clearly, transcriptional control of Swe1 synthesis is not necessary for a working morphogenesis checkpoint, but the length of the delay depends sensitively on the level of Swe1 expression. This sensitivity is even more evident in *cdc24<sup>ts</sup> SWE1-2X* and *cdc24<sup>ts</sup> SWE1-4X* mutants (McMillan et al., 1999a), where ND occurs much later (over 5 h in both cases) than in *cdc24<sup>ts</sup>* (135–165 min; Sia et al., 1996, 1998). Actually, the system is sensitive to the ratio of Mih1 to Swe1 rather than to the absolute value of Swe1 expression, as shown in an elegant experiment by Sia et al. (1996). They altered systematically the Mih1/Swe1 ratio by creating diploid strains (*MIH1-mih1* and *mih1-mih1*) in a background homozygous for *SWE1* and *cdc24<sup>ts</sup>*. They repeated the same experiment, this time altering *SWE1* dosage in a diploid strain homozygous for *MIH1* and *cdc24<sup>ts</sup>*. In these four mutants, the delay of ND is shown to increase with the ratio of active Swe1 to active Mih1 (Sia et al., 1996). We simulate these and other mutants in two stages: first with the checkpoint turned off (*cdc24<sup>ts</sup>* at 25°C) and then with the checkpoint turned on (*cdc24<sup>ts</sup>* at 37°C).

### Checkpoint inactive (permissive temperature)

**wild type, *mih1 $\Delta$* , and *hsl1 $\Delta$* .** Although Swe1 is able to phosphorylate Cdc28–Clb2 and it is transcribed earlier than Clb2, the morphogenesis checkpoint is not operational during normal cell division. How does the model explain this apparent contradiction? Fig. 3 shows that, as soon as bud formation occurs, most of the active Swe1 is modified by Hsl1 into Swe1M and therefore inactivated. Cdc28–Clb2 rises rapidly and phosphorylates Swe1M, converting it into PSwe1M, which is rapidly degraded. The time course of total Swe1 (Swe1T) agrees with published data (Sia et al.,

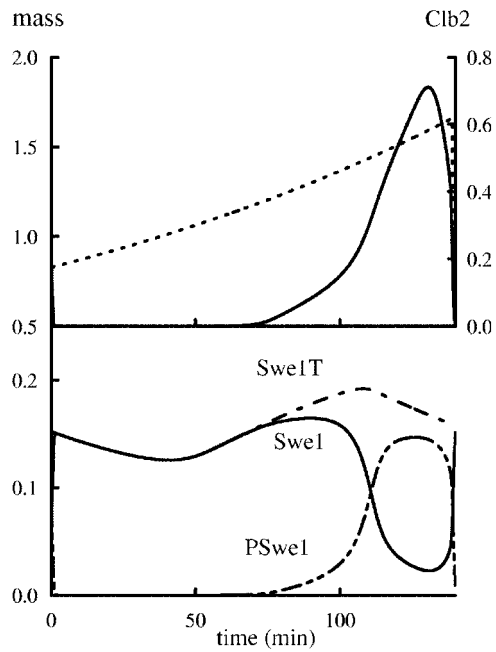


Figure 4. ***hsl1Δ* cells.** (Parameter values as in Table S2, except for alterations specified in row 4 of Table I.) Mass and Cdc28–Clb2 dynamics (top, dotted and solid lines, respectively) resemble closely the wild-type cycle, whereas Swe1 dynamics is different (bottom) because Swe1 cannot be modified by Hsl1.

1998). Concentration of the phosphorylated unmodified form (PSwe1) is negligible during a wild-type cell cycle, according to the model. A similar timing of Swe1 redistribution among its four forms occurs in *mih1Δ* (unpublished data), because Swe1 never gets a chance to phosphorylate Cdc28–Clb2. On the other hand, in *hsl1Δ* (Fig. 4), Swe1 follows a completely different path in the Swe1 box (Fig. 2). Because the left part of the box is unavailable, Swe1 oscillates between its active form and its phosphorylated form. Total Swe1 undergoes small amplitude oscillations because Cdc28–Clb2 transiently inhibits its transcription factor, SBF, but it does not undergo large amplitude oscillations, as in wild type and *mih1Δ*, because Swe1 is never transformed into the highly unstable form (PSwe1M) in *hsl1Δ* (McMillan et al., 1999a). Although this redistribution of Swe1 among its four possible forms is completely different from wild type and *mih1Δ*, the overall timing of cell division is not affected. Even though Cdc28–Clb2 is inhibited, it accumulates enough active form to switch on its transcription, to activate Mih1, and eventually to phosphorylate and inhibit Swe1.

***mih1Δ clb2Δ* compared to *hsl1Δ clb2Δ*.** The different roles of Hsl1 and Mih1 become even more evident in the double mutant cells *mih1Δ clb2Δ* and *hsl1Δ clb2Δ*. Even though the single mutants, *mih1Δ* and *hsl1Δ*, are very similar, the double mutants with *clb2Δ* are not; *hsl1Δ clb2Δ* showing a more severe phenotype (longer cells) than *mih1Δ clb2Δ* (Lew, D.J., personal communication). In our model, Clb1 and Clb2 are lumped together as Clb2. Based on evidence in Cross et al. (2002), we assume that Clb2 transcription accounts for two thirds of the total Clb1 + Clb2 transcription, whereas Clb1 transcription is the remaining one third. Hence, in *clb2Δ* we reduce Clb transcription rate

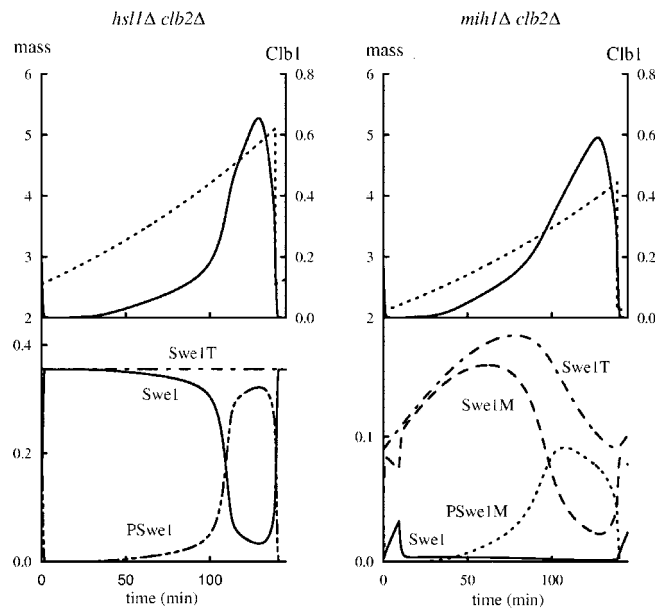


Figure 5. **Comparison of *hsl1Δ clb2Δ* and *mih1Δ clb2Δ*.** (Parameter alterations specified in rows 7 and 8 of Table I.) Both cells grow larger than wild-type cells (top: dotted line is mass, solid line is Cdc28–Clb1), but *hsl1Δ clb2Δ* cells are 21% larger than *mih1Δ clb2Δ*. The Swe1 dynamics explains the different behavior: in *mih1Δ clb2Δ* the delay is only due to *CLB2* deletion, whereas in *hsl1Δ clb2Δ*, Swe1 also contributes to Cdc28–Clb1 inhibition. Notice that total Swe1 does not oscillate in *hsl1Δ clb2Δ* because mass is big enough (as measured by Cln-dependent kinase activity) to keep SBF always active (not depicted).

( $k_{s,clb}$ ) to one third of its wild-type value. In our simulation, we get similar qualitative results (Fig. 5): *hsl1Δ clb2Δ* cells are 21% larger than *mih1Δ clb2Δ* cells. The reason why *mih1Δ clb2Δ* shows a less severe phenotype is that Hsl1 creates inactive Swe1M. This way, even though only Clb1 is transcribed, it is enough to lead the cell into mitosis. On the other hand, in *hsl1Δ clb2Δ*, there is a battle between Swe1 and Cdc28–Clb1, which is initially won by Swe1 because it is transcribed first. Clb1 transcription is initially kept low, the cell is stuck in G2 and increases in size. However, an increasing amount of Clb1 accumulates in the nucleus as the cell becomes larger, and eventually it is able to transform Swe1 to its inactive phosphorylated form PSwe1, and to lead the cell through mitosis.

***mih1Δ hsl1Δ*.** It is known that either Hsl1 alone or Mih1 alone is sufficient to help Cdc28–Clb2 against Swe1, whereas the double mutant is inviable. In the model, we obtain a similar result (Fig. 6). Comparing the double mutant with *hsl1Δ* (Fig. 4), we see that, without any help from Mih1 and Hsl1, Cdc28–Clb2 is unable to win against Swe1. As a result, the cell is blocked in G2; it grows very large and dies.

### Checkpoint active (restrictive temperature)

***cdc24<sup>ts</sup>, cdc24<sup>ts</sup> hsl1Δ, and cdc24<sup>ts</sup> mih1Δ*.** At the restrictive temperature, *cdc24<sup>ts</sup>* cells are similar to *hsl1Δ mih1Δ*, but not as extreme, because we assume that Mih1 preserves 10% of its activity when the checkpoint is invoked. As a result, ND is delayed, giving rise to dinucleated cells (ND but not cell division). ND timing in the simulation is compara-

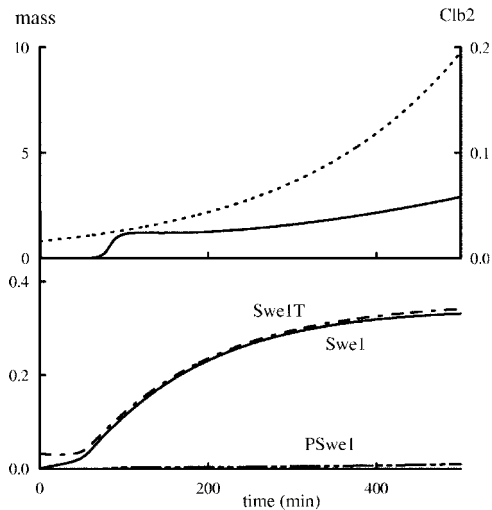


Figure 6. *hsl1Δ mih1Δ* cells. (Parameter alterations specified in row 5 of Table I.) Mass and Cdc28–Clb2 (top, dotted and solid lines, respectively) increase during the G2 arrest, until the cell dies (Other rules). G2 block is due to active Swe1, which represents the largest fraction of the total Swe1 pool (bottom).

ble to experimental observations (Table I and Fig. 7). According to the model, *cdc24<sup>ts</sup> hsl1Δ* has the same parameter set as *cdc24<sup>ts</sup>*, whereas *cdc24<sup>ts</sup> mih1Δ* shares the same parameter set with the double mutant *hsl1Δ mih1Δ* (Table I).

**GAP-SWE1 and GAL-SWE1.** Swe1 transcription is controlled by SBF, but transcriptional control is not critical for the dynamics of the system (Sia et al., 1996). To model *GAP-SWE1*, we set  $k_{s,swe} = 0$  and  $k_{s,sweC} = 0.001$ . In this case, for *GAP-SWE1* cells, ND occurs at the same time as in wild-type cells, but for *GAP-SWE1 cdc24<sup>ts</sup>* cells, ND occurs  $\sim 35$  min later. On the other hand, *GAL-SWE1* has a more severe phenotype, which can be reproduced by increasing still more the rate of *SWE1* transcription (Table I).

***cdc24<sup>ts</sup> SWE1-2X* and *cdc24<sup>ts</sup> SWE1-4X*.** To fine-tune the parameters controlling Swe1 transcription, we want to reproduce experiments where Swe1 expression is increased two- and fourfold. The simulations are again in good quantitative agreement with experimental data (Table I).

**Mih1 to Swe1 ratio in diploid cells.** This ratio is at the core of the morphogenesis checkpoint: if Swe1 (Mih1) prevails, the checkpoint is (is not) operational. Sia et al. (1996) investigated thoroughly the effect of altering the ratio in diploid strains, and discovered that ND increases with  $[Swe1]/[Mih1]$ . Simulations are in agreement with experimental data (Fig. 8). (This experiment was performed on diploid cells. We assume that the biochemical parameters are the same in the haploids and diploids, except for the transcription rates. We assume a homozygous strain AA has the same transcription rate as the haploid A, whereas transcription rate for the heterozygous Aa is one half of the haploid; Table I.)

### Parameter analysis

A thorough analysis of parameter space exceeds the aim of this work, but it is possible to investigate the behavior of the model to changes in parameter values of special biological interest (see Materials and methods). We choose not to vary

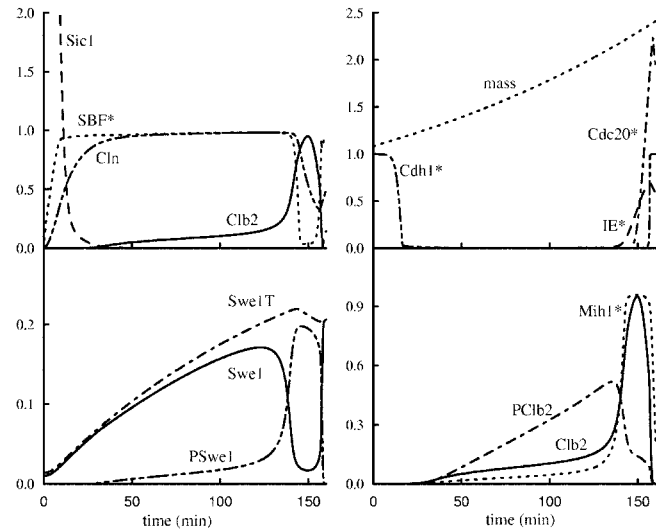


Figure 7. *cdc24<sup>ts</sup>* cells. Notice that these cells are synchronized by  $\alpha$ -factor arrest and release, and their starting size is bigger than wild-type cells. Moreover, Cln and SBF start from zero as the positive feedback loop involving Cln and SBF is switched off during synchronization by  $\alpha$ -factor. Parameters as wild type (Table S2) except for  $k_{mih} = .5$ ,  $k_{mih} = .05$ , and  $k_{hsl1} = 0$ . The asterisk identifies the more active form of a protein.

the kinetic constants of the cell cycle engine (Fig. 1) because they are based on a different set of experimental data (Tyson and Novak, 2001). Nor do we question the assumptions that Cdc28–Clb2 down-regulates Swe1 synthesis (by inactivating SBF) and up-regulates its degradation (phosphorylated Swe1 is a better substrate for ubiquitinylation), which are well founded experimentally (Sia et al., 1996, 1998). In contrast, we have made several assumptions for which there is no experimental evidence in budding yeast: that Swe1 activity is reduced by Hsl1-dependent modification and by Cdc28–Clb2-dependent phosphorylation, and that Mih1 activity is increased by Cdc28–Clb2-dependent phosphorylation. Three main questions can be formulated concerning

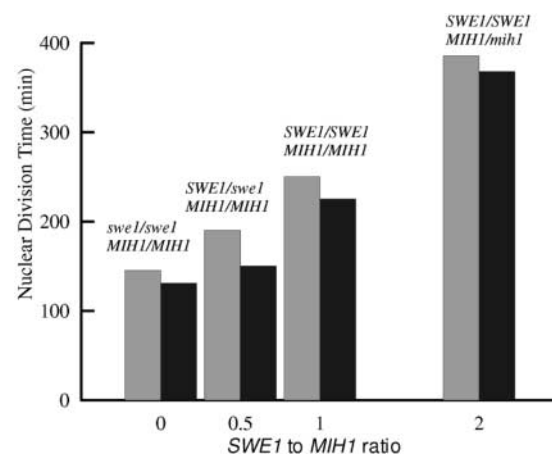


Figure 8. ND is delayed as the ratio of *SWE1* to *MIH1* increases. Gray histograms, experimental data (Table I, 9th column). Black histograms, simulated results (parameter alterations specified in rows 1, 2, 11, and 12 of Table I).

these assumptions. (1) How much activity can be given to Swe1M (rate constant  $k''_{swe}$ ) as opposed to the fully active form, Swe1 ( $k'_{swe}$ )? (2) Is Swe1 inactivation by Cdc28–Clb2 needed? In other words, what is the maximum activity that can be assigned to PSwe1 ( $k'''_{swe}$ )? (3) Is Mih1 activation by Cdc28–Clb2 required? Has the activity of the nonphosphorylated form of Mih1 ( $k'_{mih}$ ) to be smaller than the activity assigned to Mih1\* ( $k'_{mih}$ )?

**Swe1M.** To determine how much Swe1M activity is tolerated by the model, we increased the rate constant  $k''_{swe}$ . The second parameter to be varied is the Mih1\* rate constant  $k'_{mih}$ , which controls the reverse reaction (dephosphorylation) on the same substrate, Cdc28–Clb2. Mih1 background rate constant  $k''_{mih}$  is set to  $k'_{mih}/10$ . Results (Fig. 9 A) show that already for  $k''_{swe} = 0.1$  (5% of Swe1 activity) it is impossible to reproduce the 13 different genotypes. Indeed, a more detailed analysis (Fig. 9 B) shows that  $k''_{swe}$  can be maximum 1.75% of  $k'_{swe}$ . Notice in Fig. 9 A that a much larger region of the parameter space (where  $k''_{swe}$  reaches 20% of  $k'_{swe}$ ) fits 12 genotypes, the missing one being always due to the fact that the size of *clb2Δ hsl1Δ* fails to exceed the size of *clb2Δ mih1Δ*. This is not surprising, because as soon as some activity is given to Swe1M, it becomes harder for Cdc28–Clb2 to overcome Swe1 in *clb2Δ mih1Δ* mutants, whereas it has no effect on *clb2Δ hsl1Δ* where Swe1M is not present. We conclude that these unpublished data put a severe constraint on the activity of Swe1.

**PSwe1 and Mih1.** A second two-parameter analysis was performed to investigate the requirements of activation of Mih1 by Cdc28–Clb2 and inactivation of Swe1 by Cdc28–Clb2. First, we want to know whether Swe1 inactivation alone can be sufficient. The positive feedback between Cdc28–Clb2 and Mih1 is eliminated by assigning the same activity to Mih1 and Mih1\* (i.e.,  $k'_{mih} = k'_{mih}$ ). Their common value is the first parameter to be varied. The second parameter is  $k'''_{swe}$ , the activity assigned to PSwe1, whereas Swe1 activity ( $k'_{swe}$ ) is kept constant. As  $k'''_{swe}$  approaches  $k'_{swe} = 2$  (Table S2), Swe1 regulation disappears. If any combination of these two parameters can fit all 13 genotypes, we conclude that, for those particular parameter values, the positive feedback loop between Mih1 and Cdc28–Clb2 is not needed. As shown in Fig. 9 C, such a parameter region exists.

Second, we are interested in the possibility that neither the positive feedback between Cdc28–Clb2 and Mih1 nor the negative effect of Cdc28–Clb2 on Swe1 is present. This possibility indeed exists for  $k'_{mih} = k'_{mih} = 1.5$  and  $k'''_{swe} = k'_{swe} = 2$  (Fig. 9 C).

In Fig. 9 D, we show that when both Swe1 and Mih1 are regulated (the two parameters varied in this analysis are  $k'_{swe}$  and  $k'_{mih}$ , whereas  $k''_{swe} = k'_{swe}/10$  and  $k''_{mih} = k'_{mih}/10$ ), the model is consistent with the data on all 13 genotypes for  $k'_{mih}/k'_{swe} \approx 1.5$ . Parameter analysis (unpublished data) reveals that this region of consistency is  $\sim 50\%$  larger than in the completely unregulated model (i.e.,  $k'_{mih} = k'_{mih}$  and  $k''_{swe} = k'_{swe}$ ). For this reason, we prefer a model in which both Swe1 and Mih1 activities are affected by phosphorylation by Cdc28–Clb2. In addition, this preference is consistent with known properties of Swe1 and Mih1 homologues in fission yeast (Tang et al., 1993) and *Xenopus laevis* (Izumi et al., 1992).

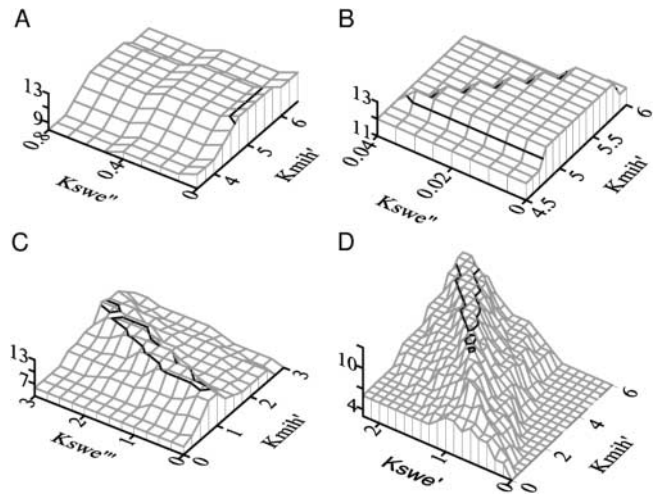


**Figure 9. Parameter analysis.** The number of successfully simulated genotypes (to within  $\pm 20\%$  of experimental results) changes with parameter values. Each node of the grids corresponds to a simulation run. Black contour lines (at level 12.5) encircle regions of parameter space where all 13 genotypes have been successfully simulated. (A) The activity of Swe1M,  $k''_{swe}$ , is varied against the activity of Mih1\*,  $k'_{mih}$ . (B) Enlargement of A. (C) PSwe1 kinase activity  $k'''_{swe}$  is varied simultaneously with unregulated Mih1 activity  $k'_{mih} = k'_{mih}$ . (D) Both Swe1 and Mih1 are regulated,  $k'_{mih} = k'_{mih}/10$  and  $k''_{swe} = k'_{swe}/10$ .

Summarizing, parameter analysis shows that, for our model to be consistent with the data in Table I, Swe1M has to be less active than Swe1, but phosphorylation-dependent inactivation of Swe1 and activation of Mih1, although present in the model, can be relaxed.

## Discussion

When bud formation is impaired, the morphogenesis checkpoint delays ND to allow for a bud to be formed. The molecular mechanism underlying this G2 delay relies on the antagonism between Swe1 and Cdc28–Clb2. These two protein kinases inhibit each other, and engagement of the checkpoint depends on the outcome of their fight. During a normal cell cycle, Cdc28–Clb2 is able to overcome Swe1 activity, whereas when bud formation is impaired, Swe1 is stabilized and active, and the cell cycle is delayed in G2 phase. The morphogenesis checkpoint inhibits the activity of Cdc28–Clb2 in two different ways. First, because bud formation is impaired, Hsl1 cannot act to inhibit Swe1 and to label it for degradation. Moreover, if actin cannot polymerize, then a second inhibitory signal impinges on the cell cycle through a MAPK pathway, whose ultimate effect is to alter the ratio of activities of Mih1 and Swe1 (by inactivating Mih1, or possibly by activating Swe1). Reviewing the current literature, we have formulated a hypothesis (wiring diagram) of the way these genes and proteins interact.

The main objective of our analysis is to verify whether the proposed mechanism can reproduce in quantitative detail the relevant experimental data. Because intuition and qualitative arguments are inadequate to predict the behavior of the complex network controlling yeast cell cycle dynamics (Fig. 1) and the morphogenesis checkpoint (Fig. 2), we have tried to put this problem in a rigorous mathematical context.

### Model's assumptions

The molecular network controlling yeast cell cycle dynamics has been studied in detail (Chen et al., 2000), and the wiring diagram we use to describe it is simple but effective. On the other hand, the network we propose for the morphogenesis checkpoint is based on three assumptions that have not been experimentally verified: (1) Swe1 is inactivated when phosphorylated by Cdc28–Clb2; (2) Cdc28–Clb2 and Mih1 activate each other (a positive feedback loop); and (3) Swe1 is inactivated by a posttranslational modification introduced (indirectly) by Hsl1.

Performing a parameter analysis to investigate the extent to which these assumptions can be relaxed, we discovered that the first and second are not necessary to explain the phenotypes of the checkpoint mutants we are studying. This result is somehow surprising because assumptions 1 and 2 are based on clear experimental evidence in *X. laevis* and *S. pombe*. It is possible that these assumptions will be needed in the future, when more experiments characterizing the morphogenesis checkpoint must be taken into account. We decided to include them in the basal parameter set, because of analogies with other organisms and because these assumptions make the model more robust.

As for the third assumption, parameter analysis shows that it cannot be relaxed. In particular, D.J. Lew (personal communication) showed that *clb2Δ hsl1Δ* cells are larger than *clb2Δ mih1Δ* cells. This observation poses a strict constraint on the activity of Swe1M, the Hsl1-modified form. Were this constraint ignored, the other data in Table I would permit a larger activity for Swe1M. Nonetheless, even without this constraint some regulation of Swe1M activity is required, as other genotypes fail when Swe1M activity reaches 20% of Swe1 activity. Summarizing, our model predicts that Hsl1 indirectly inactivates Swe1 activity.

The size difference between *clb2Δ hsl1Δ* and *clb2Δ mih1Δ* plays a crucial role in constraining parameter values of the model. For the basal parameter set we propose, *clb2Δ hsl1Δ* cells are only 21% larger than *clb2Δ mih1Δ* cells. The size differential cannot be made much larger without bringing the model into contradiction with some other property of the mutant set. Most parameter changes away from the basal set reduce the size differential and quickly bring the model's prediction below our acceptance threshold (size ratio >1.15). Given the importance of this observation in constraining the model, we suggest that the size ratio of these two mutants be measured accurately.

### Model's behavior

According to the model, Swe1 can be present in four different forms, and the way Swe1 is distributed among these forms depends on whether the checkpoint is invoked or not. In wild-type cells, the morphogenesis checkpoint is normally switched off because as soon as the bud is formed Hsl1 is activated and Swe1 is converted into the inactive form, Swe1M. If *HSL1* is deleted, the unmodified Swe1 is able to phosphorylate and inactivate Cdc28. In this case, dephosphorylation of Cdc28 (i.e., the presence of Mih1) becomes necessary. On the other hand, if *MIH1* is deleted, Swe1 can still be converted into the doubly modified form (PSwe1M) and degraded. This basic difference between *mih1Δ* and

*hsl1Δ* is particularly evident in the double mutants *clb2Δ hsl1Δ* and *clb2Δ mih1Δ*. These cells experience a G2 delay because they rely on Clb1 alone to enter mitosis. In *hsl1Δ clb2Δ* the delay lasts longer than in *mih1Δ clb2Δ*, because Swe1 cannot be converted into its modified inactive form Swe1M. Not surprisingly, when both *HSL1* and *MIH1* are deleted, the cell is blocked in G2.

These behaviors set the stage for understanding the morphogenesis checkpoint. A *cdc24<sup>ts</sup>* cell has a similar, but milder, phenotype than a *mih1Δ hsl1Δ* cell, as we assume that the signal transduction pathway operating through Mpk1 does not completely inhibit Mih1. Therefore, the G2 block in *mih1Δ hsl1Δ* becomes a G2 delay in *cdc24<sup>ts</sup>*. After a time the checkpoint-induced cell (*cdc24<sup>ts</sup>*) undergoes adaptation, i.e., ND without bud formation. The selective advantages of this control loop are clear: becoming dinucleate is to be avoided, if possible, but it is better than death.

### Bifurcation diagrams

The morphogenesis checkpoint acts like a “governor” to the cell cycle engine, slowing progression through the cell cycle when a particular danger signal (failure to bud) is perceived. To understand the relationship between the engine and its governor, it is useful to introduce the notion of a bifurcation diagram. In Fig. 10, we plot Cdc28–Clb2 activity (the state of the engine) as a function of cell size (the motive force for cell cycle progression in yeast; see Bifurcation analysis, available at <http://www.jcb.org/cgi/content/full/jcb.200306139/DC1>; Tyson et al., 2001, 2002). Under normal conditions (Fig. 10 A), the Cdc28-control system has two characteristic states: a stable steady state (at small size) and a stable oscillatory state (at large size). A small newborn cell is attracted to the stable steady state of low Cdc28–Clb2 activity; kept low by active Cdh1 and Sic1 (Fig. 1). The cell is trapped in G1 because it is too small to warrant a new round of DNA replication and division. When the cell grows to a critical size (Fig. 10 A, mass = 1), the stable steady state is lost, and the cell cycle engine begins an oscillation that drives Cdc28–Clb2 to larger activity. The cell replicates its DNA and enters mitosis. The mitotic state is intrinsically unstable, because high levels of Cdc28–Clb2 turn on Cdc20, which destroys Cdc28's cyclin partner. As Cdc28 activity drops, the cell divides and the control system is reset to the domain of the stable steady state. The duration of the budded phase (S-G2-M) is fixed at ~60 min, the time it takes to complete one oscillation. The duration of G1 phase is variable, depending on growth rate and asymmetry of division.

When the morphogenesis checkpoint is invoked (no bud), active Swe1 creates a second stable steady state of the cell cycle engine at intermediate Cdc28–Clb2 activity (higher than the G1 steady state, lower than the peak of the oscillation; Fig. 10 B). Cdh1 and Sic1 are gone, Cdc28–Cln activity is high, and Cdc28–Clb2 activity is depressed by Swe1-dependent tyrosine-phosphorylation. High activity of Cdc28–Cln drives the cell into DNA synthesis, but low activity of Cdc28–Clb2 is insufficient for mitosis. Hence, the intermediate steady state corresponds to a cell stuck in G2. A newborn daughter cell will grow to mass = 1 and enter S phase, as usual. But then it arrests in G2 phase until it grows large enough to bypass the G2 arrest and enter mitosis. The delay

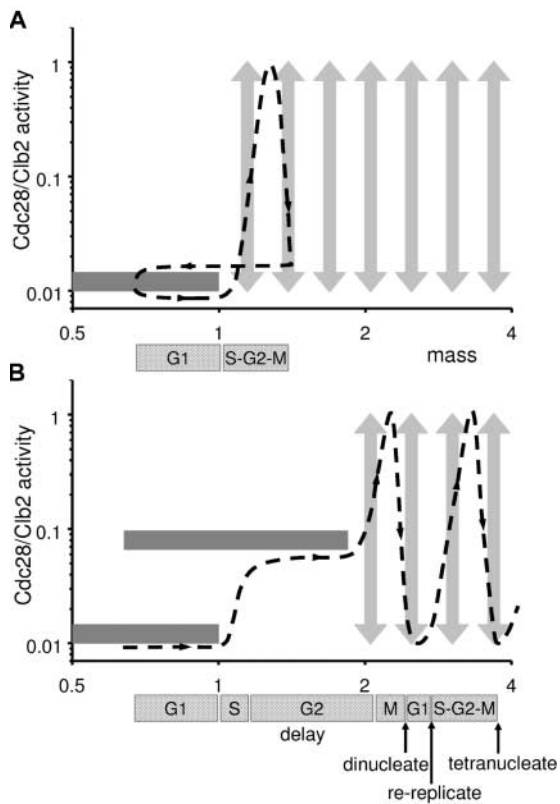


**Figure 10. Bifurcation diagrams for the cell cycle engine.** We plot Cdc28–Clb2 activity, representative of the state of the cell cycle control system, against cell mass,  $M$ , which is the driving force for progression through the cell cycle. That is, for a fixed value of  $M$ , we solve the differential equations in Table S1 until the control system reaches a stable, self-maintaining state, which is either a steady state (no further change in activities of the regulatory proteins) or an oscillatory state (perfectly repeated fluctuations of their activities). Horizontal bars are placed at the Cdc28–Clb2 level characteristic of steady states, and vertical arrows represent the range of fluctuations of Cdc28–Clb2 activity in an oscillatory state. These diagrams are schematic cartoons; for accurately computed bifurcation diagrams, see online supplemental material (Bifurcation analysis) and Fig. S1. Notice the axes are scaled logarithmically. Because we assume cells grow exponentially, equal distances along the  $\log(\text{mass})$  axis represent equal intervals of time. Along the  $\log(\text{activity})$  axis we associate low activity with G1, intermediate activity with S–G2, and high activity with M phase. (A) Checkpoint silent. The bold dashed line is a cell-cycle trajectory: as the cell grows, the Cdc28 control system is attracted to the stable, self-maintaining state at its current cell mass. A small cell persists in the G1-state until that state disappears at  $M = 1$ . Thereafter, the cell executes an oscillation in Cdc28–Clb2 activity, passing through S, G2 and M phases. When Cdc28 activity falls, as the cell exits mitosis, the cell divides and the newborn progeny are attracted to the stable G1-state. (B) Checkpoint invoked. At the restrictive temperature, a *cdc24<sup>ts</sup>* cell continues to grow but fails to make a bud. Consequently, Swe1 is stabilized, and a new self-maintaining steady state, with intermediate activity of Cdc28–Clb2, is created. The cell arrests in S–G2 phase for about one mass-doubling time, until it grows to  $M = 2$ , where the G2-arrested state disappears. At this time, the cell adapts to the checkpoint signal, enters mitosis, and becomes dinucleate. Because the cell does not divide, it stays in the oscillatory regime and rereplicates its DNA after a very short G1 phase. The cell reenters mitosis and becomes tetranucleate. The time between NDs is the period of the underlying oscillatory state,  $\sim 60$  min in the model.

will be 2–3 h, depending on growth rate and critical mass at the end of the G2-arrested state. When the cell reaches this size (Fig. 10 B, mass = 2), it adapts to the checkpoint, undergoes ND, and becomes dinucleate (the cell cannot divide because it never made a bud). At this point the model makes a noteworthy prediction. Because the engine is still in the oscillatory domain, it will pause only briefly in G1, then rereplicate its DNA and enter mitosis, becoming tetraploid (Sia et al., 1996). To see the predicted shortening of G1 phase, this experiment is best done at slow growth rates, for which the duration of G1 phase is usually long.

### Summary of the model's predictions and suggestions

The model makes two particularly clear and unexpected predictions. Regarding Hsl1 kinase, it is evidently involved in Swe1 degradation because Swe1 is stable in *hsl1 $\Delta$*  (deletion) mutants and Swe1 is degraded more rapidly in *HSL1<sup>OP</sup>* (overproduction) mutants (McMillan et al., 1999a). The effect is indirect, because Swe1 does not appear to be a substrate for Hsl1 (Cid et al., 2001). Our model calculations show that, in order to account for known dynamical features of the checkpoint mutants in Table I, Hsl1-dependent modification of Swe1 (whatever it may be) must also inhibit Swe1 kinase activity by at least 80%. To test this prediction will require reliable assays of Swe1 kinase activity, which are currently under development in Lew's laboratory (Lew, D.J., personal communication). Regarding adaptation, it is well known that *cdc24<sup>ts</sup>* cells, which cannot bud at the restrictive temperature, will nonetheless, after several hours delay, proceed through mitosis and become dinucleate. The model predicts that these cells will rereplicate their DNA soon after ND. To readily observe the predicted shortening of G1 phase, cell growth should be restricted, so that unperturbed daughter cells have a long G1 period.

The model can be used to predict mutant phenotypes (such as the many blank spaces under the E columns in Table I). Right or wrong, such predictions are handy in designing experiments and extremely valuable in interpreting the behavior of newly characterized mutants in the context of all previously studied mutants (Cross, 2003). In addition, the values assigned to most of the kinetic parameters in Table S2 are predictions. In our experience, similar predictions made on the cell cycle regulatory system of frog eggs proved to be remarkably accurate (Marlovits et al., 1998).

The model also points to other experiments that would provide critical information for refining our understanding of the morphogenetic checkpoint. For instance, first, we would like to have precise measurements of the sizes of *clb2 $\Delta$  mih1 $\Delta$*  and *clb2 $\Delta$  hsl1 $\Delta$*  cells, because these numbers would provide strict constraints on the parameters in the model. Second, we would like to know whether Cdc28–Clb2 and Mih1 are indeed involved in a positive feedback loop in budding yeast, or not. The mutant phenotypes in Table I are insufficient to resolve this issue. Third, the kinase activity of PSwe1 relative to Swe1 should be measured, to resolve the uncertainty about this ratio. Finally, for future modeling purposes, it would be nice to know whether the MAPK pathway acts by down-regulating Mih1 or up-regulating Swe1.

## Morphogenesis checkpoint or size control?

Harvey and Kellogg (2003) have recently challenged the notion of a “morphogenesis checkpoint,” claiming that Lew’s data are rather a consequence of a size control checkpoint in G2 phase of the budding yeast cell cycle. Because *swe1Δ* cells are slightly smaller than wild-type cells, they propose that wild-type budding yeast cells, like fission yeast, have a size requirement for passing from G2 into M phase, as well as a size requirement for Start (G1-S transition). Harvey and Kellogg (2003) suggest that the G2 size requirement can be met only by bud growth (not by continued expansion of the mother cell). Hence, when bud formation or growth is blocked (by the *cdc24<sup>ts</sup>* mutation or by Latrunculin-A treatment, respectively), the cell finds it difficult or impossible to meet the G2 size requirement, and so mitosis is delayed or blocked completely. In this view, there is no such thing as a morphogenesis checkpoint particular to budding yeast cells; the phenomenon is just a consequence of a minimum size for the G2-M transition and growth problems in cells that lack buds.

In Lew’s view and in our model (Fig. 10 A), the primary size requirement for wild-type cells is at Start (the G1-S transition). After passing Start, cells normally pass through S into M (without stopping in G2) and back to G1. A G2-M size requirement manifests itself only when bud formation is blocked (Fig. 10 B).

The fundamental difference between these two views is whether bud failures impair progress toward a minimum bud size for the G2-M transition (Kellogg’s view) or create a large threshold for entering into M phase (Lew’s view). Both views can explain equally well the observation that actin disruption (by treatment with Latrunculin-A) delays mitotic entry indefinitely. The two views give very different accounts of cell cycle mutants. In Lew’s picture, when a bud fails to form, a surveillance mechanism, involving Hsl1 and Mpk1, creates a stable G2-arrested steady state (Fig. 10 B), by activating Swe1 and inhibiting Mih1. The *cdc24<sup>ts</sup>* cell continues to grow at the restrictive temperature, but it must now satisfy a large size requirement for passing from G2 into M phase. After a characteristic delay, the cell enters M phase and becomes dinucleate.

In Kellogg’s picture, it is difficult to explain why *cdc24<sup>ts</sup>* cells, which fail to make a bud at all, are only delayed in entering mitosis. Why is not mitosis delayed indefinitely, as in Latrunculin-treated cells? In this case, some fraction of mother cell growth must count toward meeting the G2-M transition size. Kellogg’s view also cannot explain why *mih1Δ* causes strikingly different effects in *CDC24* and *cdc24<sup>ts</sup>* backgrounds (no delay in cell cycle progression and cell cycle block, respectively).

As we have shown by mathematical modeling, the concept of a morphogenesis checkpoint (with the assumption that Hsl1 down-regulates Swe1 activity) is compatible with most of the observed phenotypes of *cdc24<sup>ts</sup>* cells. Just like checkpoints for damaged or unreplicated DNA or for spindle defects, the morphogenesis checkpoint responds to a signal (bud failure) by arresting the cell cycle engine in a stable steady state. The arrest can be bypassed if the cell grows large enough, which is a common feature of other checkpoint mechanisms (Toczyski et al., 1997).

## Materials and methods

### Simulations

The differential equations (Table S1) were solved numerically using XPP, which is software developed by Bard Ermentrout and freely downloadable from his FTP site (<http://www.math.pitt.edu/~bard/xpp/xpp.html>). We used the CVODE integration method provided by XPP, with the default settings for the integration parameters, except relative tolerance = absolute tolerance =  $3 \times 10^{-16}$ . The model’s “.ode” file (input to XPP) is provided as on-line supplemental material (see Ciliberto\_XPP.zip), available at <http://www.jcb.org/cgi/content/full/jcb.200306139/DC1>.

### Parameter search

To investigate the sensitivity of the model to kinetic constants in the Swe1 box (Fig. 2), we chose two parameters from the box to vary simultaneously. For each pair of parameter values, we computed the model’s predictions of the data reported in Table I. Each simulated data point (call it  $R_{sim}$ , R for results) is checked against the corresponding experimental observation (call it  $R_{exp}$ ). If  $|R_{sim} - R_{exp}| / R_{exp} < 0.2$ , we assume that the simulation “fits” the experimental result, otherwise it does not.

In Table I are reported data for 14 different genotypes, the wild type plus 13 mutants. Some genotypes are characterized by more than one experimental observation: we assume that a simulated genotype fits an observed genotype only if all of its characteristics have been reproduced to within  $\pm 20\%$ . For example, in *GAP-SWE1* two conditions have to be matched: ND in cells arrested with  $\alpha$ -factor has to occur between 60 and 90 min, and ND in *cdc24<sup>ts</sup>* cells arrested in  $\alpha$ -factor has to occur between 141.6 and 94.4 min. Because we do not know precisely how much larger *clb2Δ hsl1Δ* cells are than *clb2Δ mih1Δ* cells, we assume that the simulated result is satisfactory if *clb2Δ hsl1Δ* is at least 15% larger than *clb2Δ mih1Δ*. A successful simulation should fit all 14 genotypes. Because *clb2Δ mih1Δ* and *clb2Δ hsl1Δ* are grouped together (the experimental result is the ratio of their sizes), the number of independent genotypes is 13.

Summarizing, parameter search is performed in the following way: experimental data reproduced in Table I are computed for each parameter set. Simulations are compared with experimental data for each of the genotypes. If all data characterizing a particular genotype are within  $\pm 20\%$  of experimental results, that particular genotype fits experimental data. When every genotype has been computed, a natural number in the interval [0,13] is associated with the parameter set, according to the number of genotypes that have been successfully reproduced.

### Online supplemental material

Online supplemental material includes description of the experimental basis for the model and bifurcation analysis. Also, differential equations (Table S1) and initial conditions and parameter values (Table S2) are provided. Ciliberto\_XPP.zip contains the “.ode” file of the model equations and parameter values for use with XPP, as well as .set files appropriate for each of the figures. All online supplemental material is available at <http://www.jcb.org/cgi/content/full/jcb.200306139/DC1>.

We thank Daniel Lew, Attila Csikasz-Nagy, Kathy Chen, and Jason Zwolak for much useful advice as we formulated the model, and Daniel Lew for sharing unpublished results with us.

This work has been supported by the Defense Advanced Research Project Agency (grant AFRL F30602-02-0572), the James S. McDonnell Foundation (grant 21002050), and the National Science Foundation of Hungary (grant T 032015). We thank the Collegium Budapest and the Volkswagen Stiftung for a pleasant environment in which to prepare this work for publication.

Submitted: 25 June 2003

Accepted: 30 October 2003

## References

- Amon, A., U. Surana, I. Muroff, and K. Nasmyth. 1992. Regulation of p34<sup>cdc28</sup> tyrosine phosphorylation is not required for entry into mitosis in *S. cerevisiae*. *Nature*. 355:368–371.
- Booher, R.N., R.J. Deshaies, and M.W. Kirschner. 1993. Properties of *Saccharomyces cerevisiae* wee1 and its differential regulation of p34<sup>cdc28</sup> in response to G1 and G2 cyclins. *EMBO J.* 12:3417–3426.
- Chen, K.C., A. Csikasz-Nagy, B. Gyorfy, J. Val, B. Novak, and J.J. Tyson. 2000. Kinetic analysis of a molecular model of the budding yeast cell cycle. *Mol. Biol. Cell.* 11:369–391.

- Cid, V.J., M.J. Shulewitz, K.L. McDonald, and J. Thorner. 2001. Dynamic localization of the Swe1 regulator Hsl7 during the *Saccharomyces cerevisiae* cell cycle. *Mol. Biol. Cell.* 12:1645–1669.
- Cross, F.R. 2003. Two redundant oscillatory mechanisms in the yeast cell cycle. *Dev. Cell.* 4:741–752.
- Cross, F.R., V. Archambault, M. Miller, and M. Klovstad. 2002. Testing a mathematical model for the yeast cell cycle. *Mol. Biol. Cell.* 13:52–70.
- Dirick, L., T. Bohm, and K. Nasmyth. 1995. Roles and regulation of Cln-Cdc28 kinases at the start of the cell cycle of *Saccharomyces cerevisiae*. *EMBO J.* 14:4803–4813.
- Enoch, T., and P. Nurse. 1991. Coupling M phase and S phase: controls maintaining the dependence of mitosis on chromosome replication. *Cell.* 65:921–923.
- Goldbeter, A., and D.E. Koshland, Jr. 1981. An amplified sensitivity arising from covalent modification in biological systems. *Proc. Natl. Acad. Sci. USA.* 78:6840–6844.
- Harrison, J.C., E.S. Bardes, Y. Ohya, and D.J. Lew. 2001. A role for the Pkc1p/Mpk1p kinase cascade in the morphogenesis checkpoint. *Nat. Cell Biol.* 3:417–420.
- Hartwell, L.H., and T.A. Weinert. 1989. Checkpoints: controls that ensure the order of cell cycle events. *Science.* 246:629–634.
- Harvey, S.L., and D.R. Kellogg. 2003. Conservation of mechanisms controlling entry into mitosis: budding yeast Wee1 delays entry into mitosis and is required for cell size control. *Curr. Biol.* 13:264–275.
- Izumi, T., D.H. Walker, and J.L. Maller. 1992. Periodic changes in phosphorylation of the *Xenopus* cdc25 phosphatase regulate its activity. *Mol. Biol. Cell.* 3:927–939.
- Kaiser, P., R.A. Sia, E.G. Bardes, D.J. Lew, and S.I. Reed. 1998. Cdc34 and the F-box protein Met30 are required for degradation of the Cdk-inhibitory kinase Swe1. *Genes Dev.* 12:2587–2597.
- Lew, D.J. 2000. Cell-cycle checkpoints that ensure coordination between nuclear and cytoplasmic events in *Saccharomyces cerevisiae*. *Curr. Opin. Genet. Dev.* 10:47–53.
- Lew, D.J., and S.I. Reed. 1995. A cell cycle checkpoint monitors cell morphogenesis in budding yeast. *J. Cell Biol.* 129:739–749.
- Marlovits, G., C.J. Tyson, B. Novak, and J.J. Tyson. 1998. Modeling M-phase control in *Xenopus* oocyte extracts: the surveillance mechanism for unrepliated DNA. *Biophys. Chem.* 72:169–184.
- McMillan, J.N., R.A.L. Sia, and D.J. Lew. 1998. A morphogenesis checkpoint monitors the actin cytoskeleton in yeast. *J. Cell Biol.* 142:1487–1499.
- McMillan, J.N., M.S. Longtine, R.A.L. Sia, C.L. Theesfeld, E.S.G. Bardes, J.R. Pringle, and D.J. Lew. 1999a. The morphogenesis checkpoint in *Saccharomyces cerevisiae*: cell cycle control of Swe1p degradation by hsl1p and hsl7p. *Mol. Cell. Biol.* 19:6929–6939.
- McMillan, J.N., R.A.L. Sia, E.S.G. Bardes, and D.J. Lew. 1999b. Phosphorylation-independent inhibition of Cdc28 by the tyrosine kinase swe1p in the morphogenesis checkpoint. *Mol. Cell. Biol.* 19:5981–5990.
- McMillan, J.N., L.T. Chandra, J.C. Harrison, E.S.G. Bardes, and D.J. Lew. 2002. Determinants of Swe1p degradation in *Saccharomyces cerevisiae*. *Mol. Biol. Cell.* 13:3560–3575.
- Morgan, D.O. 1995. Principles of Cdk regulation. *Nature.* 374:131–134.
- Nurse, P. 1999. Cyclin dependent kinases and regulation of the fission yeast cell cycle. *Biol. Chem.* 380:729–733.
- Russell, P., S. Moreno, and S.I. Reed. 1989. Conservation of mitotic controls in fission and budding yeast. *Cell.* 57:295–303.
- Sia, R.A.L., H.A. Herald, and D.J. Lew. 1996. Cdc28 tyrosine phosphorylation and the morphogenesis checkpoint in budding yeast. *Mol. Biol. Cell.* 7:1657–1666.
- Sia, R.A.L., E.S.G. Bardes, and D.J. Lew. 1998. Control of Swe1p degradation by the morphogenesis checkpoint. *EMBO J.* 17:6678–6688.
- Sorger, P.K., and A.W. Murray. 1992. S-phase feedback control in budding yeast independent of tyrosine phosphorylation of p34cdc28. *Nature.* 355:365–368.
- Tang, Z., Z.R. Coleman, and W.G. Dunphy. 1993. Two distinct mechanisms for negative regulation of the Wee1 protein kinase. *EMBO J.* 12:3427–3436.
- Theesfeld, C.G., T.R. Zyla, E.G. Bardes, and D.J. Lew. 2003. A monitor for bud emergence in the yeast morphogenesis checkpoint. *Mol. Biol. Cell.* 14:3280–3291.
- Toczyski, D.P., D.J. Galgoczy, and L.H. Hartwell. 1997. CDC5 and CKII control adaptation to the yeast DNA damage checkpoint. *Cell.* 90:1097–1106.
- Tyson, J.J., and B. Novak. 2001. Regulation of the eukaryotic cell cycle: molecular antagonism, hysteresis, and irreversible transitions. *J. Theor. Biol.* 210:249–263.
- Tyson, J.J., K. Chen, and B. Novak. 2001. Network dynamics and cell physiology. *Nat. Rev. Mol. Cell Biol.* 2:908–916.
- Tyson, J.J., A. Csikasz-Nagy, and B. Novak. 2002. The dynamics of cell cycle regulation. *Bioessays.* 24:1095–1109.